BBA - Biomembranes 1861 (2019) 1375–1387

Contents lists available at ScienceDirect

BBA - Biomembranes

journal homepage: www.elsevier.com/locate/bbamem

Selective antibacterial activity of the cationic peptide PaDBS1R6 against Gram-negative bacteria

Isabel C.M. Fensterseifer[a,b,1], Mário R. Felício[c,1], Eliane S.F. Alves[d], Marlon H. Cardoso[a,b,e], Marcelo D.T. Torres[h], Carolina O. Matos[d], Osmar N. Silva[e], Timothy K. Lu[f,g], Maurício V. Freire[a], Natan C. Neves[a], Sónia Gonçalves[c], Luciano M. Lião[d], Nuno C. Santos[c], William F. Porto[e,i], Cesar de la Fuente-Nunez[h,*], Octavio L. Franco[a,b,e,**]

[a] Centro de Análises Proteômicas e Bioquímicas, Pós-Graduação em Ciências Genômicas e Biotecnologia Universidade Católica de Brasília, Brasília, DF, Brazil
[b] Programa de Pós-graduação em Patologia Molecular, Universidade de Brasília, Brasília, DF, Brazil
[c] Instituto de Medicina Molecular, Faculdade de Medicina, Universidade de Lisboa, Lisbon, Portugal
[d] Laboratório de RMN, Instituto de Química, Universidade Federal de Goiás, Goiânia, GO, Brazil
[e] S-Inova Biotech, Pós-graduação em Biotecnologia, Universidade Católica Dom Bosco, Campo Grande, MS, Brazil
[f] Synthetic Biology Group, MIT Synthetic Biology Center, The Center for Microbiome Informatics and Therapeutics, Research Laboratory of Electronics, Department of Biological Engineering, Department of Electrical Engineering and Computer Science, Massachusetts Institute of Technology, Cambridge, MA, USA
[g] Broad Institute of MIT and Harvard, Cambridge, MA, USA
[h] Departments of Psychiatry and Microbiology, Perelman School of Medicine, University of Pennsylvania, Philadelphia, Pennsylvania, United States of America; Department of Bioengineering, University of Pennsylvania, Philadelphia, Pennsylvania, United States of America
[i] Porto Reports, Brasília-DF, Brazil

ARTICLE INFO

Keywords:
Antimicrobial peptide (AMP)
PaDBS1R6
Escherichia coli
Pseudomonas aeruginosa
Antibiotic resistance
Drug design
Joker algorithm

ABSTRACT

Infections caused by Gram-negative bacteria, *Escherichia coli* and *Pseudomonas aeruginosa* foremost among them, constitute a major worldwide health problem. Bioinformatics methodologies are being used to rationally design new antimicrobial peptides, a potential alternative for treating these infections. One of the algorithms used to develop antimicrobial peptides is the Joker, which was used to design the peptide PaDBS1R6. This study evaluates the antibacterial activities of PaDBS1R6 *in vitro* and *in vivo*, characterizes the peptide interaction to target membranes, and investigates the PaDBS1R6 structure in contact with mimetic vesicles. Moreover, we demonstrate that PaDBS1R6 exhibits selective antimicrobial activity against Gram-negative bacteria. In the presence of negatively charged and zwitterionic lipids the structural arrangement of PaDBS1R6 transits from random coil to α-helix, as characterized by circular dichroism. The tertiary structure of PaDBS1R6 was determined by NMR in zwitterionic dodecylphosphocholine (DPC) micelles. In conclusion, PaDBS1R6 is a candidate for the treatment of nosocomial infections caused by Gram-negative bacteria, as template for producing other antimicrobial agents.

1. Introduction

Bacterial infections have been a public health problem since the early days of civilization [1]. These infections account for a significant portion of infectious diseases, and their mortality and morbidity are currently of increasing concern worldwide [2]. The World Health Organization (WHO) has published a list of priority bacteria that are highly resistant to conventional antibiotics; novel classes of antimicrobials are needed to target these organisms. This list highlighted, as immediate threats, the *ESKAPE* pathogens, which include carbapenem-resistant *Acinetobacter baumannii*, carbapenem-resistant *Pseudomonas aeruginosa*, carbapenem-resistant and extended-spectrum beta-lactamase (ESBL)-producing *Enterobacteriaceae* [3–5]. Despite the growing public health threat posed by antibiotic resistance, the number

* Correspondence to: C. de la Fuente-Nunez, Departments of Psychiatry and Microbiology, Perelman School of Medicine, University of Pennsylvania, Philadelphia, Pennsylvania, United States of America; Department of Bioengineering, University of Pennsylvania, Philadelphia, Pennsylvania, United States of America.
** Correspondence to: O.L. Franco, Centro de Análises Proteômicas e Bioquímicas, Programa de Pós-Graduação em Ciências Genômicas e Biotecnologia, Universidade Católica de Brasília SGAN, Quadra 916, Módulo B, Av. W5 Norte, CEP 70.790-160 Brasília, DF, Brazil.
E-mail addresses: cfuente@pennmedicine.upenn.edu (C. de la Fuente-Nunez), ocfranco@gmail.com (O.L. Franco).
[1] These authors contributed equally to this work.

https://doi.org/10.1016/j.bbamem.2019.03.016
Received 17 December 2018; Received in revised form 8 March 2019; Accepted 24 March 2019
Available online 26 March 2019

of new antibiotics approved by the FDA has been decreasing annually [6], partly a reflection of the waning interest by pharmaceutical companies to invest in anti-infective therapies, and partly an indication of the multiple obstacles that arise during the process of approving substances with this potential [7,8].

Antimicrobial peptides (AMPs) represent promising alternatives to classical therapies to target infections [9]. In general, they have an amphipathic and cationic structure, with a positive net charge between +3 and +9, ranging in size from 12 to 50 amino acid residues [1,10–12]. Other desirable properties when developing a drug are broad-spectrum activity, so that several kinds of pathogenic bacteria are targeted, and multifunctionality, so that antibiofilm, antiviral, antifungal or anticancer properties are included in the drug's spectrum of activity [13–15].

In the process of drug development, the rational design is one of the first steps [9,11], and during this, hundreds or even thousands molecules have been developed, and a few functional hits are often identified based on the original design rules [16], to be tested in a more in-depth manner. We recently developed the Joker algorithm for rational peptide design, a method that is based on inserting rigid patterns onto peptide sequences through a sliding window system, generating a new analogue for each on [17]. In the initial screening, 84 peptides with predicted antimicrobial activity were generated and subsequently tested against a *Pseudomonas aeruginosa* luminescent strain [17]. PaDBS1R6 (PMARNKKLLKKLRLKIAFK) was one of the peptides designed using the Joker algorithm, based on the parent peptide PaDBS1 [17], a ribosomal fragment from the archaeum *Pyrobaculum aerophilum*. PaDBS1 was selected among other candidates because of its potent antimicrobial activity during the screening process.

Here, we demonstrate that the peptide PaDBS1R6 exhibited selective antimicrobial activity against Gram-negative bacteria, as it lacked activity against the Gram-positive bacteria strains tested. Experiments with lipid vesicles showed that the interaction of PaDBS1R6 with negatively charged and zwitterionic lipids induced a change in the structure of the peptide from random coil to α-helix conformation, characterized both by circular dichroism (CD). The tertiary structure was determined by nuclear magnetic resonance (NMR). In view of these results, we suggest that the peptide could be a candidate that could be developed to treat the nosocomial infections caused by Gram-negative bacteria or to be used as a template for designing new antimicrobial agents.

2. Material and methods

2.1. Peptide synthesis

The peptide PaDBS1R6 was synthesized by Peptide 2.0 (USA) using the fluorenylmethyloxycarbonyl chloride (Fmoc) strategy in solid phase. The peptide was purified by reverse-phase HPLC using an analytical C_{18} column (Phenomenex, USA). Molecular mass and purity of the synthesized peptide were confirmed by MALDI-ToF mass spectrometry [18] (Fig. S1).

2.2. Formation of large unilamellar vesicles

LUVs with a diameter of ~100 nm were obtained by extrusion of multilamellar vesicles (MLVs), as described elsewhere [19]. 1-Palmitoyl-2-oleoyl-*sn*-glycero-3-phosphocholine (POPC), 1-palmitoyl-2-oleoyl-*sn*-glycero-3-phosphoethanolamine (POPE) and 1-palmitoyl-2-oleoyl-*sn*-glycero-3-phospho-(1′*sn*-glycerol) (POPG) were obtained from Avanti Polar Lipids (Alabaster, AL, USA). Cholesterol (Chol) and cardiolipin (CL) were obtained from Sigma (St. Louis, MO, USA). The LUVs studied were zwitterionic (pure POPC and POPC:Chol (70:30)) or anionic (POPC:POPG (70:30) and POPE:POPG:CL (65:30:05)), mimicking membrane systems relevant for the study [20]. Stock solutions of different compositions in MLVs were kept at 4 °C overnight before measurements, and MLVs were extruded the day of the measurement. HEPES buffer (10 mM HEPES, 150 mM NaCl, pH 7.4) was used in all the measurements, except when otherwise indicated.

2.3. Preparation of bacterial cells for confocal microscopy

E. coli ATCC 25922 was maintained as stock cultures at −80 °C and revived by plating in Luria-Bertani (LB) agar (CONDA, Madrid, Spain) overnight at 37 °C. An isolated bacterial colony was used to inoculate LB broth, and the culture was allowed to grow overnight at 37 °C. 200 μL of culture were used to freshly inoculate 10 mL of LB. The suspension was then allowed to grow at 37 °C for ~3 h, until it reached log-phase, with a final bacterial concentration of $\sim 1 \times 10^8$ colony-forming units per mL (CFU mL^{-1}) (optical density at 600 nm, OD_{600} ~0.257). Bacteria were then centrifuged three times for 25 min at 4000 × *g* and resuspended in buffer or broth with a final determination of the cell concentration [21].

2.4. Animals

Female C57BL/6 mice (6 to 8 weeks-old) were provided by the Central Bioterium of USP/Ribeirão Preto, São Paulo, Brazil, and female CD-1 mice (6 weeks-old) were bought from Bharles River (Boston, MA). C57BL/6 mice were housed and euthanized according to Silva *et al.* [22].The procedures with C57BL/6 and the care and handling of the animals were approved by the Ethics Committee of the Catholic University of Brasilia (030/15). CD-1 mice were maintained in accordance with the Guide for the Care and Use of Laboratory Animals in an Association for Assessment and Accreditation of Laboratory Animal Care International (AAALAC) accredited facility. All procedures were approved by MIT's Institutional Animal Care and Use Committee (IACUC), protocol number 1016-064-19.

2.5. Hemolytic assay

The hemolytic activity of PaDBS1R6 was determined by using fresh C57BL/6 mouse red blood cells (mRBCs). Cells were separated from the plasma by sedimentation and then washed three times with a 0.15 M NaCl and 0.01 M Tris-HCl, pH 7.4 solution. After that, erythrocytes were resuspended in phosphate buffered-saline (PBS), pH 7.4. With the aid of a polyethylene tube, several concentrations of the sample were incubated with 50 μL of mRBCs suspension for 1 h at 37 °C. The negative and positive controls were PBS and Triton X-100, respectively. Tubes were then centrifuged at 12,000 ×*g* for 15 s, 100 μL of the supernatant was added to the multi-well plate, and readings were carried out at 405 and 567 nm in an ELISA reader (Bio-Tek Power Wave HT, USA) [23].

2.6. Antibacterial assays

Minimum inhibitory concentrations (MICs) of PaDBS1R6 against *Escherichia coli* (ATCC 8739, ATCC 25922, KPC+ 001812446 and KPC+ 3789319), *Klebsiella pneumoniae* (ATCC 13883 and KPC+ 3259271), *P. aeruginosa* (ATCC 27853, PAO1 and PA14), *Staphylococcus aureus* (ATCC 25923) and methicillin-resistant *S. aureus* (clinical isolate 713623) were determined by the standardized dilution method, according to NCSLA guidelines [24]. Initially, a single colony of each bacteria was inoculated in Mueller Hinton broth (MH) (Himedia, India) or Basal Medium 2 (BM2) and incubated for 18 h, at 37 °C and 200 rpm. Overnight cultures were transferred to new MH and incubated at 37 °C until they reached exponential phase (OD_{595} ~0.7). Then, cultures were adjusted to a final concentration of 1×10^6 CFU mL^{-1}, using the equation previous described [25]. MICs were measured using PaDBS1R6 from 2 to 64 μM per well. Bacteria in medium and chloramphenicol were used as negative and positive controls, respectively. Plates were incubated at 37 °C for 24 h. The MIC was defined as the lowest tested concentration that led to complete inhibition (100%) in comparison to the negative-control group [22].

2.7. In vitro selectivity index

The *in vitro* selectivity index (SI) is the ratio between the cytotoxic and antibacterial activity. The selectivity index of PaDBS1R6 was calculated using Eq. (1) [26]:

$$SI = \frac{Hemolysis}{\sqrt[n]{\prod_{i=1}^{n} Antibacterial_i}} \tag{1}$$

where n corresponds to the number of antimicrobial assays with different biological samples. For activity values higher than the maximum concentration tested, the concentration value added to the equation was assumed to be two-fold the maximum tested value (*e.g.*, if the value was higher than 100, it was considered as 200) [26].

2.8. Anti-biofilm screening assays

Biofilms of *P. aeruginosa* strain PAO1 were grown in the absence or presence of PaDBS1R6 (16 μM) according to Reffuveille *et al.* [27]. Microscopy was performed using a confocal laser scanning microscope (Zeiss LSM 700 Laser Scanning Confocal), and three-dimensional reconstructions were generated using the Imaris software package (Bitplane AG). Two independent replicates were performed for each group.

2.9. Confocal microscopy

A confocal laser point-scanning microscope Zeiss LSM 880 (Carl Zeiss, Germany), with airyscan, equipped with HE GFP 450–490 nm and HE DsRed 538–562 nm lasers, was used to obtain images of bacteria cells. Images were taken on 35 mm, low, ibiTreat μ-dishes (reference 80136, ibidi, Madison, WI, USA), with an EC Plan-NeoFluar 20× objective. Bacteria cells were analyzed using the same kit from biofilm assays. Images were acquired with Zen 2 software (dark edition, Carl Zeiss, Germany).

2.10. Atomic force microscopy

E. coli cells were prepared as described above. Bacteria were incubated at 25 °C for 1 h, control and treated samples were incubated in the absence and presence of peptide (7 μM), respectively. Procedure and conditions are described by Migliolo *et al.* [28,29]. Images were analyzed with the JPK image processing software v. 5.1.13.

2.11. Murine intraperitoneal infection model

C57BL6 mice received an intraperitoneal injection of 100 μL of *E. coli* ATCC 8739 containing 1×10^8 CFU.mL^{-1}. One hour after the infection, mice (5 mice per group) were treated intraperitoneally with PaDBS1R6 at concentrations of 5 or 10 mg kg^{-1}, gentamicin (10 mg.kg^{-1}, positive control), or PBS (negative control) for four days [22]. Mice were euthanized at day 4 post-infection; peritoneal fluid was collected and bacterial CFUs were counted. Serial dilutions of the homogenates were plated in triplicate on MH, and the results were expressed as CFU.mL^{-1} [30].

2.12. Scarification skin infection mouse model

P. aeruginosa strain PA14 was grown and used to infect the skin scarification made on the back of the CD-1 mice according to Pane *et al.* [31]. The concentration used for single dosage of the peptide was 64 μM. Two independent experiments were performed with 4 mice per group in each condition. Statistical significance was assessed using a one-way ANOVA followed by Bonferroni's test: ***$p < 0.001$ compared to untreated group.

2.13. Dynamic light scattering and zeta-potential

Dynamic light scattering (DLS) experiments were carried out using a Malvern Zetasizer Nano ZS (Malvern, UK), with backscattering detection at 173°, equipped with a He-Ne laser (632.8 nm), using disposable cuvettes at 25 °C, as described elsewhere [32]. Normalized intensity autocorrelation functions were analyzed using the CONTIN method [33], yielding a distribution of diffusion coefficients (D). The measured D was used to calculate the hydrodynamic diameter (D_H) through the Stokes-Einstein relationship. A set of 15 measurements (with 10 runs each) for the liposomes were done in the absence and presence of the different concentrations of the peptide. The zeta-potential (ξ) of the liposomes was determined at 25 °C from the mean of 15 measurements (100 runs each), in the absence and presence of different peptide concentrations, using disposable zeta cells DTS 1060 (Malvern, UK) with gold electrodes, after 15 min of equilibration time [34]. Values of viscosity and refractive index were set at 0.8872 cP and 1.330, respectively. The lipid concentration used was the same as that in the DLS assays in order to acquire high enough count rates [34,35]. All results were processed using the Malvern DTS software, after three independent experiments.

2.14. Fluorescence spectroscopy assays

2.14.1. Labeling with di-8-ANEPPS

LUVs were prepared as described above, using the same lipid compositions. After extrusion, the lipid vesicles were diluted to 500 mM for labeling and incubated overnight at 25 °C with 10 μM of di-8-ANEPPS for maximum dye incorporation. This dye provides information about the differences induced by the peptide in the membrane dipole potential. Lipid at 200 mM and 1 μM of the dye was used for the measurements. To label *E. coli* cells, after cell washing, 10^5 CFU mL^{-1} of cells were incubated with 100 μM of the dye and HEPES buffer with 0.05% (w/v) of Pluronic F-127, for 1 h at 25 °C with gentle agitation and protection from the light. The suspensions were prepared at a final concentration of 10^4 CFU mL^{-1} of bacteria and 10 μM of the dye. Prior to the measurement, the solutions were incubated with peptide for 1 h (until 15 μM). Excitation spectra and the ratio of intensities were obtained at the excitation wavelengths of 455 and 525 nm ($R = I_{455}/I_{525}$). Emission was set at 670 nm to avoid membrane fluidity-related artefacts [36–38]. Excitation and emission slits for these measurements were set to 5 and 10 nm, respectively. The variation of the ratio with the peptide concentrations was analyzed by a single binding site model using Eq. (2):

$$\frac{R}{R_0} = 1 + \frac{{}^{R_{min}}\!/_{R_0} \cdot [Peptide]}{K_d + [Peptide]} \tag{2}$$

where the R value is normalized by R_0, the value in the absence of peptide. R_{min} defines the asymptotic minimum value of R, and K_d is the dissociation constant [39]. Experimental data fitting was performed by non-linear regression with GraphPad Prism 6. Error bars represent the standard deviation of three replicates.

2.14.2. Labeling with Laurdan

LUVs were labeled by adding Laurdan to a final probe concentration to reach a molar ratio of 1:300 (3 mM of lipid concentration and 9.90 μM of probe). The mixture was incubated in the dark for 30 min at 25 °C. To label the bacterial cells, after cell washing and determination of cell density, bacteria were incubated with 10 μM of the dye at a final concentration of 10^4 CFU.mL^{-1}. This mixture was also incubated in the dark for 30 min at 25 °C. Laurdan emission spectra (between 400 and 600 nm) were measured after 1 h of incubation in the absence and presence of different concentrations of the peptide, with excitation at

350 nm, and bandwidths of 5 and 10 nm for excitation and emission, respectively. To quantify the spectral changes, Laurdan generalized polarization (G_p) was calculated as follows in Eq. (3) [40]:

$$G_p = \frac{I_{440} - I_{490}}{I_{440} + I_{490}} \quad (3)$$

where I_{440} and I_{490} are the emission intensities at 440 nm and 490 nm (corresponding to the gel and liquid crystalline lipid phases), respectively. Assays were done in three replicates, and error bars represent standard deviation.

2.14.3. Fluorescence anisotropy

LUVs were prepared as described above, using the same lipid compositions. LUVs (3 mM lipid concentration) were incubated with DPH or TMA-DPH to achieve a final probe concentration of 0.33 mol%. After the addition of the fluorescence probes, all samples were protected from the light to avoid photobleaching and maintained at 25 °C, for 30 min with gentle agitation. *E. coli* cells were labeled after determining the cell concentration and diluting them to 10^4 CFU mL^{-1} in HEPES buffer, with 10 µM of the dyes. The incubation was also for 30 min at 25 °C, with gentle agitation and protection from the light. The different peptide concentrations were also incubated for 1 h (until 15 µM). Steady-state fluorescence anisotropy, ⟨r⟩, was calculated as demonstrated in Eq. (4):

$$\langle r \rangle = \frac{I_{VV} - G.\, I_{VH}}{I_{VV} + 2 \cdot G \cdot I_{VH}} \quad (4)$$

where I_{VV} and I_{VH} are the parallel and perpendicular polarized fluorescence intensities measured with the vertically polarized excitation light, and $G = I_{HV}/I_{HH}$ is a correction factor accounting for the polarization bias of the detection system. For DPH, excitation and emission wavelengths were 350 and 432 nm, respectively, whereas for TMA-DPH, excitation was at 355 nm and emission was at 430 nm [41]. All the assays were done in three replicates, and error bars represent standard deviation.

2.15. Circular dichroism

CD measurements were carried out in a JASCO J-815 spectropolarimeter (Tokyo, Japan), using quartz cuvettes of 0.1 and 0.5 path length. Spectra were acquired between 190/200 and 260 nm, at 25 °C, with data pitch of 0.5 nm, wavelength sampling velocity of 50 and 200 nm min^{-1}, and data integration time of 1 s with at least 5 accumulations. Measurements to determine the peptide secondary structure in different media and pH values were performed with a PaDBS1R6 concentration of 50 µM. Media included 20 mM of dodecylphosphocholine (DPC) micelles and 20 mM of sodium dodecyl sulfate (SDS), at pH 4.0 (2 mM sodium acetate buffer), pH 7.0 (2 mM Tris-HCl buffer), and pH 10.0 (2 mM glycine-NaOH buffer). Deionized water was also used as control medium. Lipid vesicles were titrated in PBS (10 mM sodium phosphate, 150 mM NaCl) at pH 7.4, with different lipid concentrations up to 1.5 mM, with and without 16 µM of PaDBS1R6. In addition to blank subtraction, experimental instrument-related baseline drift was corrected by subtracting from all spectra the average of the signal between 250 and 260 nm. Spectra were normalized to mean residue molar ellipticity (θ, deg cm^2 $dmol^{-1}$). All conditions were measured independently and in triplicate [42]. To integrate the structural information, the ellipticity signal at 222 nm was also plotted as a function of the lipid concentration. The effect of the various lipid compositions tested was then evaluated through the different parameters obtained, using Eq. (5):

$$\Delta\theta_{222\ \mathrm{nm}} = \frac{\Delta\theta_{222\ \mathrm{nm\ max}} \cdot [Lipid]}{K_D^{app} + [Lipid]} \quad (5)$$

where the $\Delta\theta_{222\ \mathrm{nm}}$ is the difference of the PaDBS1R6 signal in the presence and absence of lipid, $\Delta\theta_{222\ \mathrm{nm\ max}}$ is the maximum ellipticity value obtained from the fitting and $K_D{}^{app}$ is the half-maximal effect that represents the apparent dissociation constant [43]. The fitting of the experimental data using this equation was done by non-linear regression with GraphPad Prism 6. Error bars represent standard deviation of the three replicates.

2.16. NMR spectroscopy and structure calculations

For NMR experiments, the peptide was prepared by dissolving 2 mM in 0.6 mL of aqueous solution of H_2O/D_2O (9:1) and 200 mM perdeuterated DPC-d_{38}, sodium phosphate buffer 1 mM at pH 7.0. Hydrogen chemical shifts were expressed with respect to sodium 2,2-dimethyl-2-silapentane-5-sulfonate (DSS, 0.05 mM), as an internal chemical shift standard for ^{1}H NMR spectroscopy. Two-dimensional NMR homonuclear ^{1}H-^{1}H TOCSY and NOESY, heteronuclear ^{1}H-^{13}C HSQC, and ^{1}H-^{15}N HMQC experiments were obtained from natural abundance, on a Bruker Avance 600 spectrometer. TOCSY data points were obtained using a mixing time of 80 ms and NOESY with 100, 150, 200 and 250 ms. All contour maps were processed by NMRPipe [44] and analyzed using NMRViewJ [45]. Full sequential assignment was achieved using the general strategy described by Wüthrich [46]. The structure calculations were performed using the simulated annealing protocol in the XPLOR-NIH software [47]. NOEs were converted into semi-quantitative distance, derived from the NOE intensities. The dihedral angle restraints (φ and ψ) of the protein backbone was predicted by program TALOS+ [44]. Two hundred structures were calculated, and the lowest 20 energy conformers were selected and submitted to a water refinement protocol. The ensemble of the 10 lowest energies represented the solution structural ensemble of PaDBS1R6. This final ensemble of accepted structures was selected based on the following criteria: no NOE violations > 0.3 Å, rmsd for bond deviations from ideality < 0.05 Å, and rmsd for back dihedral angle violations < 5°. The coordinates of the PaDBS1R6 have been deposited in Protein Data Bank (PDB ID: 6CFA).

2.17. Solvation potential energy calculation

The solvation potential energy was measured for the 10 lowest energy NMR structures. Each structure was separated into a single PDB file. The PDB files were converted into ".pqr" files by the utility PDB2PQR using the AMBER force field [48]. The grid dimensions for Adaptive Poisson-Boltzmann Solver (APBS) calculation were also determined by PDB2PQR. Solvation potential energy was calculated by APBS [49]. Surface visualization was performed using the APBS plugin for PyMOL.

3. Results

3.1. PaDBS1R6 targets Gram-negative bacteria

In order to test the antimicrobial activity of PaDBS1R6, minimal inhibition concentration assays (MIC) were performed against Gram-negative and -positive antibiotic-susceptible and antibiotic-resistant bacterial strains (Figs. 1A and 2B, Table S1). The peptide was active against all Gram-negative bacterial strains tested, with MIC values ranging from 8 µM against *E. coli* and *P. aeruginosa* strains (Figs. 1A and 2A) to 16 µM against carbapenem-resistant *K. pneumoniae* (Table S1). Moreover, the peptide showed activity (64 µM) against the Gram-positive bacteria tested (susceptible *S. aureus* and methicillin-resistant *S. aureus* with MIC for the peptide of 64 µM and > 64 µM, respectively - Table S1). In an attempt to improve its antibacterial activity, the peptide was combined (see supplementary methods) with the antibiotics tetracycline or cefotaxime and tested against carbapenem-resistant *K. pneumoniae*. No synergistic activity was detected against this species (Table S2).

We next sought to complement the *in vitro* and *in vivo* activity

A

Organism	PaDBS1R6 MIC (µM)
Pseudomonas aeruginosa ATCC 27853	16
Pseudomonas aeruginosa Pa14	8
Pseudomonas aeruginosa PAO1	8

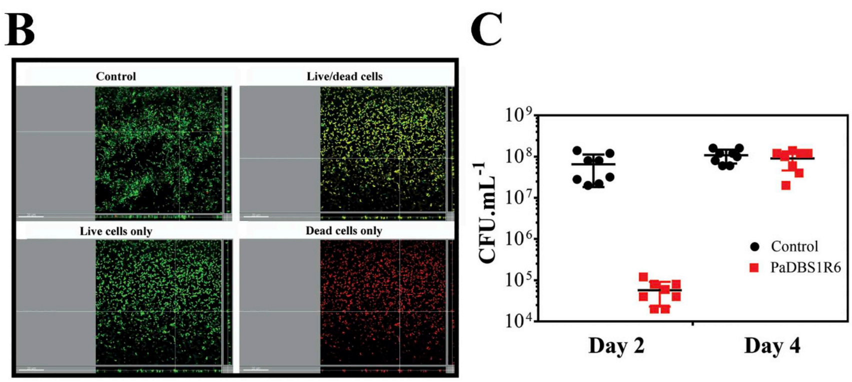

Fig. 1. PaDBS1R6 activity against *P. aeruginosa*. (A) Minimum inhibitory concentration of PaDBS1R6 against *P. aeruginosa strains*. (B) Flow cell analysis of *P. aeruginosa* PAO1 biofilm formation in the absence and presence of 16 µM of PaDBS1R6. *P. aeruginosa* biofilms were cultivated in minimal medium for 48 h in the presence of 16 µM of peptide at 37 °C in flow chambers. Biofilms were imaged by widefield fluorescence microscopy, using SYTO9 to stain live cells (green fluorescence) and propidium iodide (PI, red fluorescence), a normally cell-impermeable stain, to stain compromised cells. The scale bar represents 15 µm, and each panel shows xy, yz, and xz dimensions. (C) Recovery of bacterial load of the wound from female CD-1 mice infected with *P. aeruginosa* PA14 after 2 and 4 days of infection. The wound was inoculated with ~5×10^6 CFU of bacteria and treated with PaDBS1R6 (64 µM). Values represent the mean ± SD and data were analyzed by one-way ANOVA and Bonferroni test: ***$p < 0.001$ compared to untreated group.

studies by determining the therapeutic profile of PaDBS1R6. In this work, the selectivity index was calculated for the peptide using Eq. (1). Hemolytic assays showed that PaDBS1R6 did not compromise red blood cells at the tested concentrations (> 87 µM). Thus, considering the MICs against Gram-negative bacteria and the hemolysis assessments, PaDBS1R6 showed a selectivity index of 17.85, demonstrating that for the peptide to be toxic, a dose 17-fold higher than that required for antimicrobial activity would have to be present.

3.2. Antimicrobial activity against P. aeruginosa planktonic cells and pre-formed biofilms

In order to demonstrate the peptide activity toward *Pseudomonas* spp., several assays were performed. Anti-*Pseudomonas* spp. activity was assessed *in vitro* against *P. aeruginosa* PA14 and PAO1 (8 µM), and against *P. aeruginosa* ATCC 27853 (16 µM) (Fig. 1A). The antibiofilm activity of the peptide was also tested, showing that PaDBS1R6 treatment reduced biofilm volume (Fig. 1B). PaDBS1R6 *in vivo* efficacy was evaluated using a scarification skin infection mouse model. Single dose treatment with PaDBS1R6 (64 µM) decreased the bacterial load by ~10^3 CFU mL^{-1} ($p < 0.001$) two days after treatment (Fig. 1C). This promising activity, however, was not observed after 4 days of infection, when both untreated and PaDBS1R6-treated animals presented higher bacterial loads at the site of infection (~10^8 CFU mL^{-1}).

3.3. Effect of PaDBS1R6 treatment on the viability and morphology of E. coli cells

E. coli planktonic cells viability after exposure was assessed using a live/dead kit that labels viable cells green and membrane compromised bacterial cells red [50]. Images of the effects of PaDBS1R6 at concentrations of 7 and 15 µM (MIC and 2-fold MIC) were acquired after 1 h of incubation (Fig. 2B). Microscopy confirmed the results obtained, as peptide at the lower concentration damaged > 50% of the *E. coli*

A

Organism	PaDBS1R6 MIC (µM)
Escherichia coli ATCC 8739	8
Escherichia coli ATCC 25922	8
Carbapenem-resistant *Escherichia coli* 3789319	8

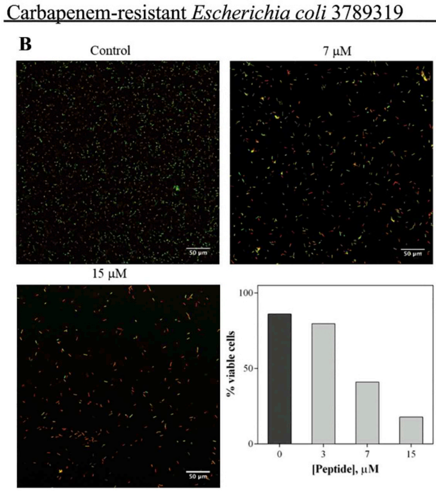

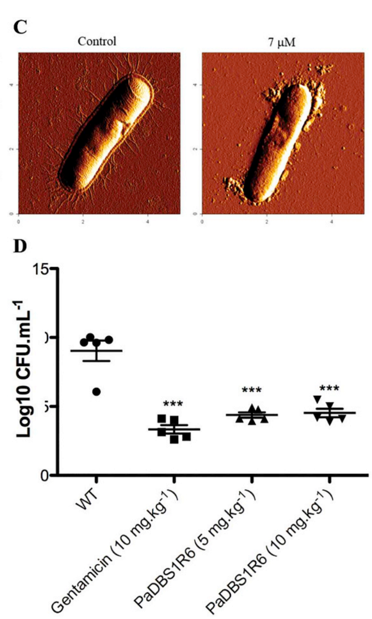

Fig. 2. PaDBS1R6 activity against *Escherichia coli*. (A) Minimum inhibitory concentration of PaDBS1R6 against *E. coli* strains. (B) Fluorescence confocal microscopy images of *E. coli* cells in the absence (control) and presence of PaDBS1R6 (7 and 15 µM). Images are representative of one assay, with SYTO9 and PI dyes being used for identification of viable and membrane compromised cells, respectively. Percentage of viable cells calculated from confocal fluorescence microscopy images, using FIJI (ImageJ), by comparing the number of green stained cells relatively to the total number present. Values represented were calculated for the images presented. (C) Atomic force microscopy images of *E. coli* cells in the absence (control) and presence of PaDBS1R6 (7 µM), with 1 h of incubation. Total scanning area of $5 \times 5\,\mu m^2$. (D) Female CD-1 mice infected with ~1×10^8 CFU of *E. coli* ATCC 8739 and treated *i.p.* with PaDBS1R6 (5 and 10 mg.kg^{-1}), gentamicin (10 mg.kg^{-1}) or PBS 1 h after infection. The injections were repeated after 24 h for 3 days. Values represent the mean ± SD and data were analyzed by one-way ANOVA and Bonferroni test: ***$p < 0.001$ compared to untreated group.

cells (Fig. 2B). When the peptide concentration was increased, PaDBS1R6 treatment led to nearly 80% compromised cells.

To further confirm the antimicrobial activity of PaDBS1R6 against *E. coli*, we used AFM to evaluate possible morphological damage of bacterial membranes caused by PaDBS1R6 (7 μM). As expected, the untreated controls were viable with no membrane deformaton. On the contrary, bacterial samples treated with PaDBS1R6 showed increased membrane roughness and cytosol leakage in both apical regions (Fig. 2C).

Considering the efficiency displayed by PaDBS1R6 against *E. coli*, and to further assess the potential of this agent as a novel drug, we tested its efficacy in an *in vivo* intraperitoneal infection model. We defined a pattern of non-lethal infection that has been previously described [30]. Mice were infected with *E. coli* ATCC 8739 *via* intraperitoneal (*i.p.*) injection, and 1 h later were treated *i.p.* with 5 or 10 mg.kg^{-1} of peptide or 10 mg.kg^{-1} of gentamicin (Fig. 2D). Seventy-two hour post-infection, peritoneal fluid was collected and bacterial CFU were counted. The number of viable bacterial cells in the peptide-treated groups significantly decreased, from 10^{10} to 10^4 CFU mL^{-1}. Although two different doses of the peptide were tested, there was no significant difference between these groups, as they both reduced bacterial counts by 6 orders of magnitude, to 10^4 CFU mL^{-1}. Additionally, no statistical differences were observed between the gentamicin- and peptide-treated groups, which implies that PaDBS1R6 has the same efficiency at eradicating bacteria in this mouse model as the commercially available aminoglycoside antibiotic.

3.4. Evaluation of PaDBS1R6 and lipid membrane electrostatic interactions

Previous results (Fig. 2C) indicated that PaDBS1R6 could induce membrane damage. We used lipid vesicles to characterize the nature of peptide-membrane interactions and confirm these results. Initially, CD spectra of PaDBS1R6 were monitored at room temperature in the absence (Figs. S2 and S3A) and presence of four different lipid vesicle compositions (Fig. S3B, C, D and E) [42]. The peptide was evaluated in three other media: water, SDS (20 mM, pH 4.0, 7.0, and 10.0) (Fig. S2), and PBS (pH 7.4) (Fig. S3A). Vesicles were composed of POPC (Fig. S3B), POPC:POPG (70:30) (Fig. S3C), POPC:Chol (70:30) (Fig. S3D), and POPE:POPG:CL (65:30:05) (Fig. S3E). The different large unilamellar vesicles (LUVs) compositions used in this study were chosen considering the lipid composition of different cell types that could interact with the peptide, including mammalian and bacterial cells (Table 1). Considering the spectra obtained in the absence of lipid vesicles, we observed PaDBS1R6 tendency to adopt a coiled conformation in water (Fig. S2) and PBS (Fig. S3A). Equivalent results were obtained in the presence of zwitterionic lipid vesicles (Fig. S3B and C), implying that peptide-membrane interactions did not promote any structural changes under these conditions. As the lipid vesicle concentration increased, structural definition also increased in the helical minima region. In the presence of negatively charged lipid vesicles (Fig. S3D and E), which also implies an increase in hydrophobicity, PaDBS1R6 tended to adopt an α-helix structure, without full structuration.

In order to assess α-helical tendency, the ellipticity at 222 nm, a local minimum for α-helices that excludes sample polydispersity, was followed for each lipid concentration (Fig. 3A). From these data, we calculated the dissociation constants (see Materials and Methods), which provide information on peptide-membrane interaction (Table 1). For PaDBS1R6 in solution, there was no structural transition, indicated by the results obtained in the zwitterionic lipid vesicle experiments using POPC and POPC:Chol (70:30). Considering the negatively charged membranes, with the increase in lipid concentration, an increase in helix-coil transition was observed, stabilizing near 0.3 mM, implying that an electrostatic attraction is responsible for peptide-membrane interactions. These data also allowed the half maximum effects for PaDBS1R6 structural change to be determined; these effects were 61.3 ± 6.0 and 48.3 ± 7.3 μM for POPC:POPG (70:30) and inner bacterial membrane-like vesicles [POPE:POPG:CL (65:30:05)], respectively (Table 1).

Next, we used DLS in order to explore whether PaDBS1R6 promotes lipid vesicle aggregation. During these experiments, the lipid concentration was kept constant. Regarding the DLS data (Fig. 3B), increasing PaDBS1R6 concentration did not lead to the vesicles aggregates of POPC or POPC:Chol (70:30). These results are in agreement with the CD data (Fig. S3). For did not lead to vesicle agregation of POPC or POPC:Chol(70:30). There was a small increase in the hydrodynamic diameter (D_H) at higher concentrations of PaDBS1R6, but the highest aggregation profile was observed in the presence of POPE:POPG:CL (65:30:05) vesicles. These results indicate that the peptide interacts preferably with membranes that mimic the inner membrane of Gram-negative bacteria [20].

Zeta-potential studies were also performed to confirm the electrostatic destabilization that occurs for the preferably targeted membranes. The data obtained by calculating the partition coefficients (K_p) (Table 1) showed that increasing peptide concentration resulted in membrane charge destabilization only in anionic lipid vesicles, with the effect being more pronounced for inner membrane-like vesicles, corroborating the results obtained in the DLS assays (Fig. 3C). Partition coefficients obtained for POPC:POPG (70:30) and POPC:POPG:CL (65:30:05) vesicles were 2.4×10^3 and 4.8×10^3, respectively (Table 1).

3.5. Evaluation of the mechanisms of PaDBS1R6 interaction with targeted biomembranes

Experiments aimed at studying the interactions between the peptide and targeted membranes confirmed the contribution of electrostatic interactions, suggesting that PaDBS1R6 preferably interacts with anionic lipid membranes. To identify the degree of interaction, we used several membrane probes, each of which report changes in different membrane properties following peptide interactions [51,52]. For these studies, we also used zwitterionic lipid vesicles as comparative models. Studies using planktonic *E. coli* (ATCC 25922) cells were performed to

Table 1
Parameters calculated for PaDBS1R6 based on the different characterization techniques, including circular dichroism, zeta-potential and di-8-ANEPPS fluorescence spectroscopy, for each large unilamellar lipid vesicles system and *Escherichia coli* (ATCC 25922) cells.

Lipid vesicles		CD (μM)		Partition (10^3)	Di-8-ANEPPS (μM)
Composition	Mimicking systems	K_D^{app} ± SD	n ± SD	K_p ± SD	K_D ± SD
Free	–	n.d.[a]	n.d.[a]	n.a.[b]	n.a.[b]
POPC	Control	n.d.[a]	n.d.[a]	n.d.[a]	n.d.[a]
POPC:Chol (70:30)	Mammalian cells	n.d.[a]	n.d.[a]	n.d.[a]	n.d.[a]
POPC:POPG (70:30)	Simple model of Gram-negative bacteria	61.3 ± 6.0	1.56 ± 0.27	2.4	9.9 ± 1.9
POPE:POPG:CL (65:30:05)	Inner membrane of Gram-negative bacteria	48.3 ± 7.3	1.29 ± 0.26	4.8	12.4 ± 2.4
Escherichia coli (ATCC 25922)	–	n.a.[b]	n.a.[b]	n.a.[b]	n.d.[a]

n.d.[a] – data did not fit to the equation; n.a.[b] – not applicable; SD – standard deviation.

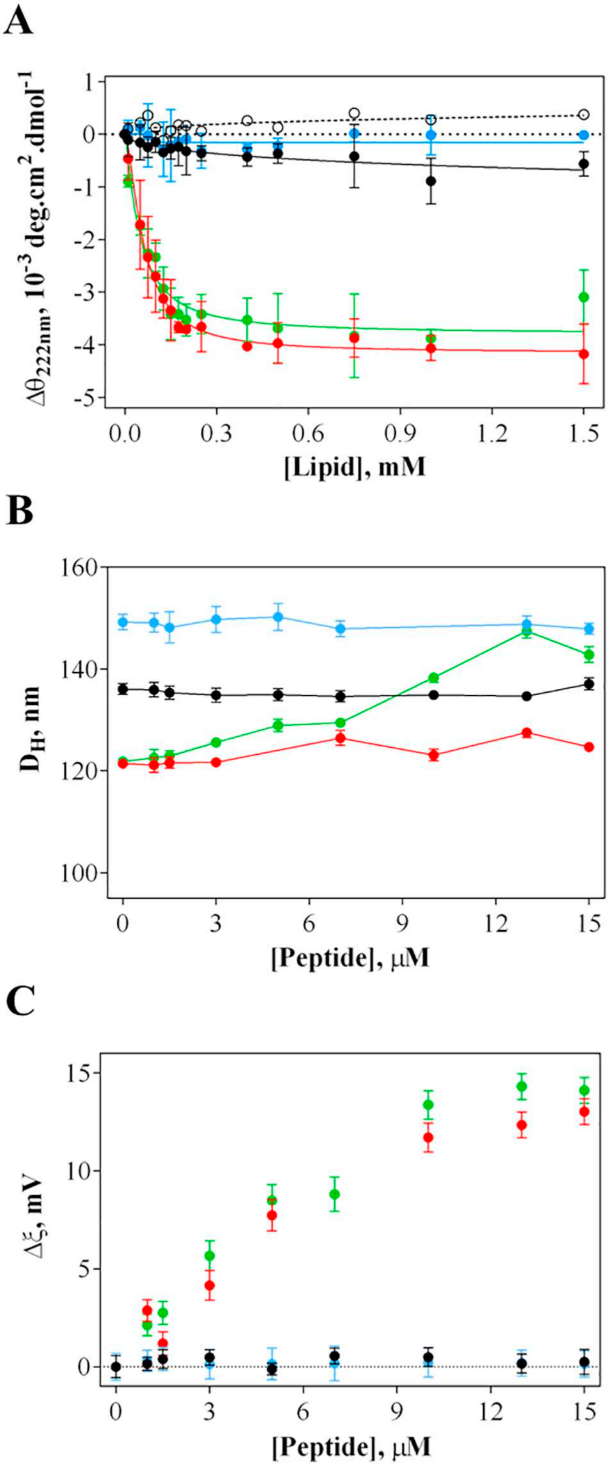

Fig. 3. PaDBS1R6 peptide-membrane interactions studied by CD, DLS and zeta-potential. (A) Comparison of the CD θ signal at 222 nm (local minimum for α-helices) for different lipid vesicle concentrations. PaDBS1R6 with a constant concentration of 16 μM (empty circles). Solid lines represent the fitting using Eq. (5). Calculated parameters are presented in Table 1. (B) DLS hydrodynamic diameter (D_H) data of the different lipid vesicles with peptide titration. Lipid concentration was kept constant at 200 μM. Solid lines represent the evolution of D_H values. (C) Zeta-potential data for the different lipid vesicles. Lipid concentration was kept constant at 200 μM upon peptide titration. Values were calculated trough the difference between the zeta-potential obtained after peptide addition and the value in the absence of peptide (initial value). From this data, partition coefficients were also calculated, using the method described elsewhere [34]. Calculated values are represented in Table 1. Lipid vesicles used included POPC (black circles), POPC:Chol (70:30) (blue circles), POPC:POPG (70:30) (red circles) and POPE:POPG:CL (65:30:05) (green circles).

gain insights into the potential *in vitro* target of PaDBS1R6. The first probe used, di-8-ANEPPS, which di-8-ANEPPS, assesses differences in the membrane dipole potential [52]. Based on the results obtained (Fig. 4A), no interaction occurred with neutral lipid vesicles, confirming once more the findings described above (Fig. 3). The dipole potential of anionic liposomes changed to a similar degree in the presence of peptide (Fig. 4A). From these results, it was possible to use Eq. (2) to calculate the K_D for the peptide-membrane interaction. For POPC:POPG (70:30) and POPE:POPG:CL (65:30:05), the K_D obtained was 9.89 ± 1.9 and 12.4 ± 2.4 μM, respectively, confirming that they have similar degrees of peptide-membrane interaction. The most extensive modification occurred in *E. coli* cells, with the first peptide concentration promoting a quick response that stagnated afterwards. This fast membrane modification may imply that PaDBS1R6 has a high affinity for the outer membrane of *E. coli* cells because of the presence of highly anionic components (*e.g.*, lipopolysaccharides, LPS) [53,54].

Next, Laurdan was used to label lipid vesicles and *E. coli* cells in order to study the differences in lipid packing and to better understand whether the peptide interacts with membranes only by electrostatic means or whether it is internalized into the membrane, where it promotes a spatial reorganization of the membrane's lipid content [55]. This information was extrapolated from the emission spectra of the dye, by calculating the generalized polarization parameter (G_p), which considers two wavelengths corresponding to the different lipid membrane phases [40]. For PaDBS1R6, either in vesicles or in *E. coli* cells, there was no significant effect, strongly indicating that no lipid reorganization occurred during peptide treatment (Fig. 4B).

To assess membrane fluidity, another important property that can be studied upon peptide interaction, the probes DPH and TMA-DPH were used, which report on membrane fluidity changes on an inner part of the membrane or closer to the lipid-water interface, respectively [41,56]. DPH inserts into the hydrophobic regions of the membrane, whereas TMA-DPH inserts close to the transition region between hydrophilic and hydrophobic media. For all lipid vesicles tested, there was no observable effect for either probe, indicating that there was no obvious membrane fluidity change (Fig. 4C and D). In *E. coli* cells, no effect was observed for TMA-DPH, but changes in fluidity were observed for DPH (a decrease of anisotropy values; Fig. 4C and D). These results indicate some loss of membrane rigidity after PaDBS1R6 treatment, being consistent with the results obtained with lipid vesicles (Fig. 3), where it was observed an increased aggregation/higher partition of the peptide for Gram-negative bacteria like vesicles (Fig. 4A and C).

3.6. PaDBS1R6 undergoes a coil-to-helix transition in the presence of hydrophobic media

The stability of the secondary structure of PaDBS1R6 was evaluated by CD, under several conditions: water, buffer (Fig. S3A), SDS micelles (Fig. S2), and DPC micelles (Fig. 5A). Water and buffer were used to determine the native structure that the peptide adopts in the absence of a target membrane. The CD spectrum of PaDBS1R6 dissolved in water or in buffer is characteristic of a random coil structure, as evidenced by a characteristic minimum at 195 nm. Literature describes this class of peptides as membrane-dependent in terms of activity, implying that in a polar protic medium environment, they tend to adopt random coil, having little defined secondary structure [32,43].

SDS micelles, an anionic detergent, were used to mimic the environment of bacterial membranes, and DPC micelles were used to mimic eukaryotic cell membranes [57]. CD analysis of PaDBS1R6 at different pH showed negative bands at 222 and 208 nm and a positive band at 193 nm, results that are consistent with well-defined helical segments. In the presence of SDS, the peptide maintained its structure (θ value at 208/222 nm is similar) in neutral and basic environments (pH 7.0 and 10.0; Fig. S2). At pH 4.0, the peptide was in its most highly structured state, as indicated by an absolute increase in signal intensity

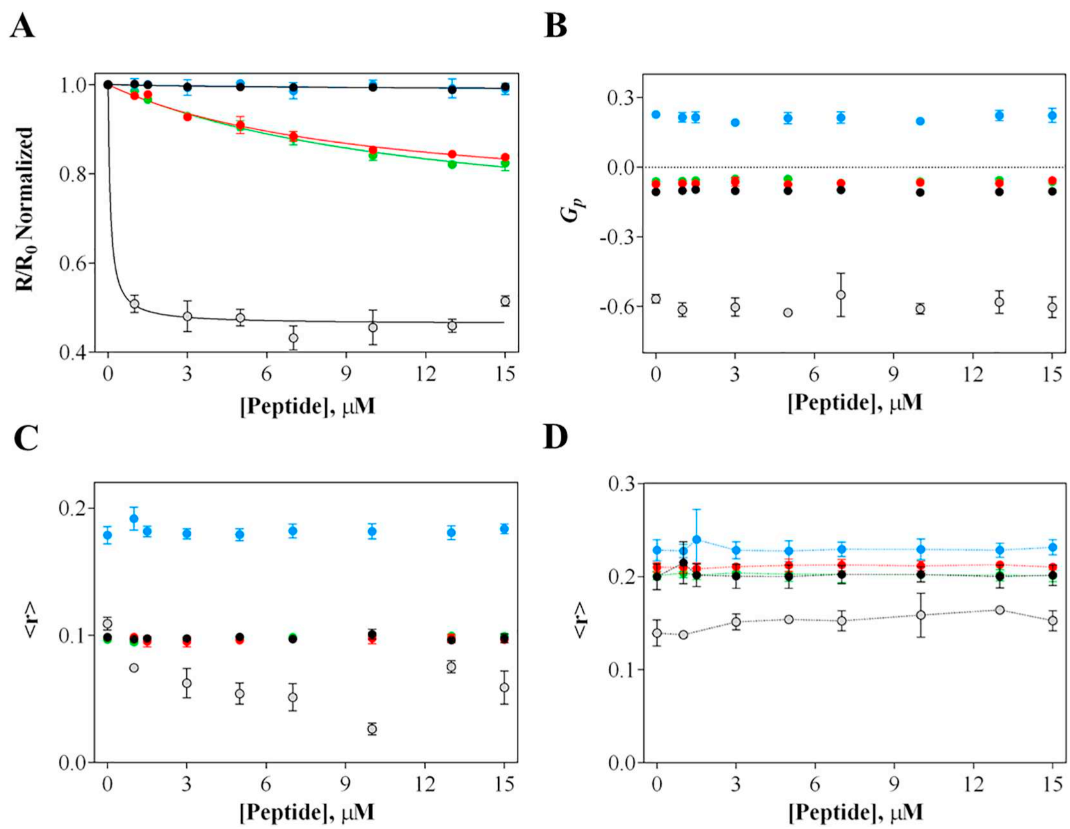

Fig. 4. Membrane dipole potential, lipid packing, and membrane fluidity studied after peptide treatment in lipid vesicles and *E. coli* cells. (A) Membrane dipole potential destabilization studied using di-8-ANEPPS. Solid lines represent the fitting using Eq. (2). Calculated parameters are presented in Table 1. (B) Generalized polarization (G_p) values obtained for the different lipid vesicles and *E. coli* cells. These measurements give information about the lipid packing. Values were calculated from the emission spectra of Laurdan using Eq. (3). (C and D) Anisotropy values obtained with DPH and TMA-DPH, respectively. These dyes give information about membrane fluidity and its changes. Values were calculated trough Eq. (4). Lipid vesicles used included POPC (black circles), POPC:Chol (70:30) (blue circles), POPC:POPG (70:30) (red circles) and POPE:POPG:CL (65:30:05) (green circles). *E. coli* cells data are represented by grey circles.

at 208 and 222 nm. In the presence of DPC micelles (Fig. 5A), the secondary structure of PaDBS1R6 was affected by the different pH levels tested. Even so, at pH 10.0, it presents higher helical content. PaDBS1R6 exhibited higher structuring at pH 10.0 and lower at pH 7.0. It is also important to mention that negatively charged lipid vesicles, as natural electrostatic targets of PaDBS1R6, also promote stabilization of the secondary structure of the peptide without being well-defined (Fig. S3B–E).

Results obtained in water and buffer were consistent with random coil conformations, contrary to the α-helical structure observed in SDS or DPC micelle environments (Figs. S2, S3A and S5A). The helix content of the PaDBS1R6 was determined from the mean residue CD at $[\theta]_{222}$ (deg cm^2 dmol^{-1}). The helix content in SDS and DPC are 31% and 28%, respectively, due the rapid inter conversion of helical and random coil segments for same peptide chain, leading to a single time-averaged resonance. Interestingly, in SDS micelles, PaDBS1R6 profile exhibited a small difference in helical pattern, compared to DPC micelles. This highlights the fact that the peptide conformation is more stable in the presence of anionic micelles and shows the role of charge in inducing peptide folding.

3.7. NMR structure of PaDBS1R6 in DPC micelles

In NMR studies, both SDS and DPC micelles are suitable membrane models because the micelles are small and have highly dynamic behavior [58]. DPC micelles have the advantage of a rapid reorientation in aqueous solution compared to the vesicle system, so they are suitable for standard high-resolution NMR studies [46]. NMR studies of the peptide in DPC-d_{38} micelles were performed using standard sequential assignment methods in combination with NOESY, TOCSY, HSQC and sf-HMQC experiments [59]. Two-dimensional (2D) NOESY experiments, acquired whit 250 ms mixing time, were used to assign the backbone and side chain resonances of the peptide, by identifying the fingerprint region with assignment of peaks (Fig. S5). The chemical shifts obtained from spectra were used as an indicator of the secondary structure [60,61]. The chemical shift index plot (Fig. S5A), calculated by NMRViewJ, showed a propensity for an α-helix formation in the region Met2-Ala17. An NOE connectivity pattern was also used to describe the secondary structure. The presence of d_{NN} (i, i + 1), $d_{\alpha\beta}$ (i, i + 3), $d_{\alpha N}$ (i, i + 3) and $d_{\alpha N}$ (i, i + 4) NOE connectivities (Fig. S5B) indicated an α-helix in the region of the amino acid residues between Asn5 and Phe18. For structural calculation, 378 NOE correlations were used, as well as 34 dihedral angle constraints derived from the TALOS analysis. The 10 lowest-energy structures, refined in water, were used for the analysis. The final 3D structure of the PaDBS1R6 peptide is presented in Fig. 5B and C. The superposition of backbone atoms from residues 2 to 17 gave a root mean square deviation (RMSD) of 0.82 ± 0.23 Å, while the superposition of all heavy atoms gave an RMSD of 1.52 ± 0.21 Å. The overall high quality of the structures was corroborated by a Ramachandran plot regarding φ and ψ angles [62], with 98.8% of the residues being present in the most favored region for α-helical structure (see Table 2 for more NMR structural statistics). Hydrophobic residues, highlighted in blue, were also identified using the lowest energy structure calculated, and include Pro1, Met2, Ala3, Leu8, Leu9, Leu12, Leu14, Ile16, Ala17, and Phe18 (Fig. 5C). The majority of hydrophobic residues were clustered on one side of the peptide structure, which indicates that PaDBS1R6 has an amphipathic character. TALOS+ predicted a helical structure between residues Ala3 and Ile16, but visual

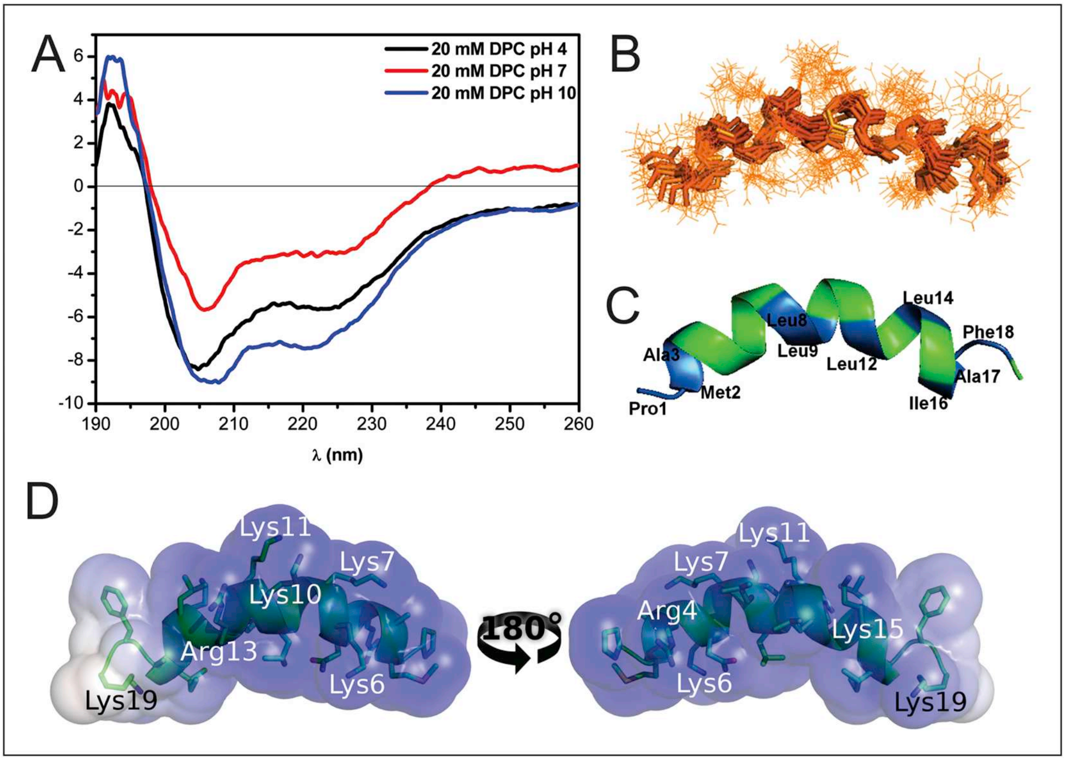

Fig. 5. CD spectra and NMR structures for PaDBS1R6. (A) Circular dichroism spectra of 50 μM PaDBS1R6 in the presence of 20 mM DPC micelles at different pH values (pH 4.0 – black, pH 7.0 – red and pH 10.0 – blue). (B) Backbone superposition of ten structures with low energy. In (C), hydrophobic and hydrophilic residues are highlighted in blue (and identified) and green, respectively. (D) Electrostatic surface of PaDBS1R6 in DPC-d38 micelles media. Surface potentials were set to ± 5 and −1 kT e−1 (133.56 mV). Blue indicates positively charged and white nonpolar ones.

Table 2
NMR structural statistics for the 10 lowest-energy structures of PaDBS1R6.

Total NOE distance restraints	378
Intra-residue	218
Sequential	104
Medium range (1 ≤ |I – j| ≤ 5)	22
Long range (|I – j| > 5)	0
Dihedral angle restraints[a]	34
Average restrictions per residue	19.9
RMSD (Å) for heavy atoms (residues 1–19)[b]	1.82 ± 0.27
RMSD (Å) backbone atoms (residues 1–19)[b]	1.05 ± 0.24
RMSD (Å) for heavy atoms (residues 2–17)[b]	1.52 ± 0.21
RMSD (Å) backbone atoms (residues 2–17)[b]	0.82 ± 0.23
Residues in favored regions on Ramachandran diagram[c]	98.8%
Residues in allowed regions on Ramachandran diagram[c]	1.2%

[a] Predicted by TALOS+ [93].
[b] Calculated by MOLMOL [94].
[c] Calculated by Ramachandran Plot Analysis (*mordred.bioc.cam.ac.uk/~rapper/rampage.php*).

analysis of the PyMOL data indicates that an α-helix is present from residues Met2 to Ala17. The electrostatic potential on the surface of the peptide structure revealed that PaDBS1R6 is highly cationic, due to its eight positively charged amino acid residues (Fig. 5D). These residues are distributed along the structure and generated a solvation potential energy of 17.33 ± 1.47 mJ mol^{-1}.

4. Discussion

The World Health Organization's list of multidrug-resistant bacteria for which novel antimicrobials are urgently needed [63], among them carbapenem-resistant and ESBL-producing bacteria (*e.g.*, *E. coli* and *P. aeruginosa*) as high-priority targets. An alternative to conventional therapies to treat drug-resistant infections is the use of AMPs. These peptides present broad-spectrum activity [64–66], and their main target has been identified as the bacterial membrane. The physicochemical properties of AMPs contribute to their ability to target bacteria and provide insight into why these agents can target not only bacteria but also fungi and cancer cells [3,11,13,15].

AMPs were originally isolated from natural sources. More recently, rational design strategies supported by advances in artificial intelligence and bioinformatics have generated AMPs with unprecedented sequences, exploring the sequence combinatorial space [17,26]. These computational methods reduce the time and cost of design and synthesis compared to the conventional methods of isolation and characterization of natural AMPs. In addition, rationally designed peptides may exhibit reduced cytotoxic activity, decreased size (which facilitates chemical synthesis), and increased antimicrobial activity [9,26].

In the last years, several methods of predicting AMP have been proposed [67]. The ADAM [68] and CAMPR3 [69] methods are designed to identify any variety of AMP. The methods of AntiBP [70] and AntiBP2 [71] concentrate on the prediction of peptides with specific activity against bacteria. Differently from these methods of prediction, the Joker algorithm is not intended to predict the antimicrobial activity of peptide, but to develop new molecules. The Joker algorithm consists of a rational design method that is based on the insertion of rigid patterns into a precursor sequence of a peptide. Prior to the use of the Joker, some sequences were selected in the NCBI Protein database according to some characteristics (presence of pattern or motif A (KK [ILV] xxx [ILVA]) and 18 amino acid residues). This search in the peptide database resulted in six sequences (EcDBS1, MmDBS1, PaDBS1, PcDBS1, PyDBS1 and TcDBS1), which were submitted to rational design using the Joker algorithm and each generated nine variants. The peptide PaDBS1R6 was one of the peptides developed by this method [17]. These peptides were first tested against bioluminescent *P. aeruginosa*. PaDBS1R6 was the peptide selected for this work because it had a promising activity against this bacterium, presenting one of the best

MICs among the molecules designed [17].

PaDBS1R6 presented a promising activity profile specifically against Gram-negative bacteria, inhibiting their growth by at least 4-fold compared to the Gram-positive strains tested. Other synthetically designed peptides have also shown activity against Gram-negative bacteria, including the DP 2–11 peptides, which were tested against *E. coli* ATCC 25922 and *P. aeruginosa* PAO1. Peptide DP 3 presented the best MIC value against *E. coli* ATCC 25922 (8 mg.L^{-1}), with DP 5, DP 7, DP 8 and DP 11 presenting the best MICs against *P. aeruginosa* (16 mg.L^{-1}) [72]. In another study, the peptide 35409 exhibited MIC values against *E. coli* ML35 and *P. aeruginosa* ATCC 15442 of 22 μM and 44 μM, respectively [26,73]. These basic activity screening tests are considered essential to initially assess AMP efficiency [28,29,74].

According to the FDA, the selectivity index indicates whether a molecule is sufficiently safe to be commercialized. The selectivity index of PaDBS1R6 was 17.85, a high value, indicative of a good drug candidate [26,75]. As the peptide did not show hemolytic activity and had a selectivity index that demonstrates its safety, we used two animal models to evaluate its biological activity. A skin infection model showed that the peptide at 64 μM reduced the number of viable *P. aeruginosa* PA14 bacteria in the treated animals after two days of infection (Fig. 1C). Previously, the same model was used to demonstrate the efficiency *in vivo* of the AMP guavanin 2 [26]. However, the peptide concentration was not sufficient to eliminate the bacterial load and not able to prevent the development of the disease later, since after 4 days of treatment the infection is again developing (Fig. 1C).

Considering that AMPs can be used for topical treatment of bacterial infections, but also in systemic infections (*i.e.*, sepsis), another *in vivo* model was tested using *E. coli* ATCC 8739 [30]. The results indicated that PaDBS1R6 was equally efficient at reducing bacterial loads in the site of infection as gentamicin, which was used as positive control. Our previous studies have also evaluated the activity of other peptides against *E. coli* using the same animal model [30,76]. Clavanin MO, a peptide modified from clavanin A, showed a reduction of bacterial load to < 10 CFU mL^{-1} [76].

As PaDBS1R6 was effective in reducing bacterial viability both *in vitro* and *in vivo*, peptide-membrane interactions and peptide structure were investigated in order to determine its structure/function relationship. Although AMPs interact first with their targets through electrostatic interactions, their actual antibacterial mechanisms are not understood in full detail [77,78]. Biophysical techniques are useful tools to track physicochemical properties that are essential for AMP mechanism of action [51]. Initially, using lipid vesicles, we established the preference of PaDBS1R6 for bacterial-like membranes constituted of POPE:POPG:CL (65:30:05), which mimic the inner membrane of Gram-negative bacteria [20,79] (Fig. 3 and Table 1). By CD and zeta-potential studies (Fig. 3A and C, respectively), we calculated the affinity and partition constants, and confirmed the preference of the peptide for negatively charged lipid vesicles that contain CL. CL, a lipid that is mostly present in the apical and septal regions of bacteria, is essential for various cellular processes [79,80]. The relevance of this membrane lipid for activity has been previously suggested for some AMP: BP100, cecropin A, and pepR [21,81]. In fact, the authors of these previous works observed that these peptides interact with CL, promoting the disruption of the bacterial membrane, the subsequent release of the cytosolic content, and finally cell death [21,81]. Our AFM data of *E. coli* treated with PaDBS1R6 (Fig. 2C) showed that cytosolic content was released near both apical regions. Moreover, studying the hydrodynamic diameter of lipid vesicles using DLS, we observed an aggregation profile in vesicles containing CL (Fig. 3B). In conclusion, in addition to the electrostatic interactions between PaDBS1R6 and negatively charged phospholipids, the presence of CL seems to be also a determinant for AMP antibacterial activity [82,83].

Next, we contributed to the understanding of mechanisms by which PaDBS1R6 acts at the membrane level by studying peptide-membrane interaction properties in lipid vesicles and *E. coli* living cells [38,51]. These studies revealed that this AMP modifies membrane dipolar potential and membrane fluidity in *E. coli* living cells, specifically within their inner membrane (Fig. 4A and C). Once more, these results highlight the dependence of PaDBS1R6 activity on a certain proportion of CL in the membrane. In fact, this activity is observed only when there is 5% CL in the vesicles, and presumably in the bacterial cell membranes as well. Gram-negative bacteria have other components in their membranes, though, that could participate in peptide activity (for the initial interactions and/or for membrane permeabilization), such as porins, lipoproteins, or teichoic acids [54,84,85]. Moreover, even when CL is present within lipid vesicles, it is not concentrated in any specific region of the liposome, contrary to what is found in bacterial cells [56,79,80].

Based on our results, PaDBS1R6 may cross the outer membrane of bacterial cells and promote inner membrane destabilization, which ultimately leads to membrane disruption and cell death. Therefore, while CL (or other membrane components) may be contributing to PaDBS1R6 action, it is important to also consider the properties of the peptide itself that may be essential for its antimicrobial activity. Positive global charge and high hydrophobic content are prototypical characteristics of this class of peptides, but their structure before and after interaction with membranes or bacterial cells can determine their affinity for membranes [3,42,86]. Initial screening of PaDBS1R6 structure stability confirmed the tendency of the peptide to adopt an α-helical conformation in highly hydrophobic media (Figs. S2 and 5A) but a random coil structure in aqueous media (Figs. S2 and S3A). In fact, as discussed above, lipid vesicles promote peptide arrangement into helical structures, with the degree of helicity correlated to the affinity of the peptide for the membranes (*i.e.*, more helical structure was observed for lipid vesicles more closely mimicking bacterial membranes. Figs. 3A and 5A). Such interactions and behaviors have been previously described for highly amphipathic AMPs, which typically have a well-defined structure after interactions with membranes, with other physicochemical properties also playing a key role in conformation flexibility and, therefore, peptide activity [87–89]. For instance, BP100 and its analogues gain structure after interacting with liposomes, specifically negatively charged ones [90]. The guavanin 2 structure, another synthetic AMP, is also stabilized after interaction with membranes, and this stability is likely to contribute to its biological function [26].

There are also examples of AMPs that lose their secondary structure upon interactions with membranes without necessarily losing their biological activity. The peptide $rBPI_{21}$ exhibited a well-defined-structure in buffer, losing it after interaction with membranes; however, in this case, structure destabilization allowed the insertion of the peptide in the targeted membranes, thus contributing to its function [91]. The difference between PaDBS1R6 and $rBPI_{21}$ can be explained by the particular amino acid sequence: the insertion of the hydrophobic amino acids of PaDBS1R6 into the bacterial membrane depends on a rearrangement of its conformation (Fig. 5B–D). In order to understand what happens to the structure of PaDBS1R6 when the peptide interacts with membranes, NMR structural studies were performed in the presence of DPC micelles (Fig. 5B–D). PaDBS1R6 has an amphipathic structure and highly cationic net charge, with the hydrophobic amino acid residues disposed on one side of the α-helical structure. These results indicate that, once electrostatic interactions have occurred, the careful rearrangement of the residues is what allows the peptide to insert into the membrane.

5. Conclusions

In summary, our study indicates that in the presence of vesicles composed of bacterial-like membranes, the conformation of PaDBS1R6 turns from random coil to α-helix. Our investigations show that during the peptide-membrane interaction, PaDBS1R6 is structured in an amphipathic α-helix, which binds at membrane interfaces first by electrostatic interactions between the cationic peptide and the anionic head-groups of lipids in the membrane and, secondly, by hydrophobic interactions between the hydrophobic face of the peptide and the membrane [92]. This folding from random coil in solution to an ordered conformation proved to be strongly dependent on the nature of the lipid bilayer. We have demonstrated the antibacterial selectivity of PaDBS1R6 against Gram-negative bacteria *in vitro* and *in vivo* in two different infection models and we demonstrate the safety of this peptide for use in animals by calculating its selectivity index. The findings of the present study suggest that PaDBS1R6 is a selective antimicrobial peptide for Gram-negative bacteria, and as such, a candidate template for the development of new antimicrobial agents.

Conflict of interest statement

TKL is a co-founder of Senti Biosciences, Synlogic, Engine Biosciences, Tango Therapeutics, Corvium, BiomX, and Eligo Biosciences. TKL also holds financial interests in nest.bio, Ampliphi, and IndieBio.

Transparency document

The Transparency document associated with this article can be found in the online version.

Acknowledgements

This work was supported by Fundação para a Ciência e a Tecnologia – Ministério da Ciência, Tecnologia e Ensino Superior (FCT-MCTES, Portugal) project PTDC/BBB-BQB/3494/2014, Marie Skłodowska-Curie Research and Innovation Staff Exchange (MSCA-RISE, European Union) project INPACT (call H2020-MSCA-RISE-2014, grant agreement 644167), Ramon Areces Foundation (to CFN), DTRA (HDTRA1-15-1-0050 to TKL), Fundação de Amparo à Pesquisa do Estado de São Paulo (FAPESP #2016/24413-0 to MDTT), Fundação de Amparo à Pesquisa do Estado de Goiás (FAPEG # 201710267000062 to ESFA) and Fundação de Apoio à Pesquisa do Distrito Federal (FAPDF). MRF acknowledges FCT-MCTES fellowship SFRH/BD/100517/2014. ONS holds a postdoctoral scholarship from National Council of Technological and Scientific Development (CNPq) and Fundação de Apoio ao Desenvolvimento do Ensino, Ciência e Tecnologia do Estado de Mato Grosso do Sul (FUNDECT) – Brazil [300583/2016-8]. MHC acknowledges fellowship 141518/2015-4 (CNPq) and 88881.134423/2016-01 (CAPES).

Appendix A. Supplementary data

Supplementary data to this article can be found online at https://doi.org/10.1016/j.bbamem.2019.03.016.

References

[1] O.N. Silva, K.C.L. Mulder, A.E.A.D. Barbosa, A.J. Otero-Gonzalez, C. Lopez-Abarrategui, T.M.B. Rezende, S.C. Dias, O.L. Franco, Exploring the pharmacological potential of promiscuous host-defense peptides: from natural screenings to biotechnological applications, Front. Microbiol. 2 (2011) 232, https://doi.org/10.3389/fmicb.2011.00232.
[2] J. Lueangsakulthai, N. Jangpromma, T. Temsiripong, J.E. McKendrick, W. Khunkitti, S.E. Maddocks, S. Klaynongsruang, A novel antibacterial peptide derived from *Crocodylus siamensis* haemoglobin hydrolysate induces membrane permeabilization causing iron dysregulation, oxidative stress and bacterial death, J. Appl. Microbiol. 123 (2017) 819–831, https://doi.org/10.1111/jam.13539.
[3] B. Gomes, M.T. Augusto, M.R. Felício, A. Hollmann, O.L. Franco, S. Gonçalves, N.C. Santos, Designing improved active peptides for therapeutic approaches against infectious diseases, Biotechnol. Adv. 36 (2018) 415–429, https://doi.org/10.1016/j.biotechadv.2018.01.004.
[4] M.J. Llewelyn, J.M. Fitzpatrick, E. Darwin, C. Sarahtonkin-Crine, J. Gorton, T.E.A. Paul, L. Peto, S. Yardley, A.S. Walker Hopkins, The antibiotic course has had its day, BMJ 358 (2017), https://doi.org/10.1136/bmj.j3418.
[5] S. Vasoo, J.N. Barreto, P.K. Tosh, Emerging issues in Gram-negative bacterial resistance: an update for the practicing clinician, Mayo Clin. Proc. 90 (2015) 395–403, https://doi.org/10.1016/j.mayocp.2014.12.002.
[6] M. May, Drug development: time for teamwork, Nature 509 (2014) S4–S5, https://doi.org/10.1038/509S4a.
[7] R. Tommasi, D.G. Brown, G.K. Walkup, J.I. Manchester, A.A. Miller, ESKAPEing the labyrinth of antibacterial discovery, Nat. Rev. Drug Discov. 14 (2015) 529–542, https://doi.org/10.1038/nrd4572.
[8] J. Rello, E. Bunsow, A. Perez, What if there were no new antibiotics? A look at alternatives, Expert. Rev. Clin. Pharmacol. 9 (2016) 1547–1555, https://doi.org/10.1080/17512433.2016.1241141.
[9] W.F. Porto, Á.S. Pires, O.L. Franco, Antimicrobial activity predictors benchmarking analysis using shuffled and designed synthetic peptides, J. Theor. Biol. 426 (2017) 96–103, https://doi.org/10.1016/J.JTBI.2017.05.011.
[10] O.N. Silva, W.F. Porto, S.M. Ribeiro, I. Batista, O.L. Franco, Host-defense peptides and their potential use as biomarkers in human diseases, Drug Discov. Today (2018), https://doi.org/10.1016/J.DRUDIS.2018.05.024.
[11] M.R. Felício, O.N. Silva, S. Gonçalves, N.C. Santos, O.L. Franco, Peptides with dual antimicrobial and anticancer activities, Front. Chem. 5 (2017) 5, , https://doi.org/10.3389/fchem.2017.00005.
[12] C. de la Fuente-Núñez, O.N. Silva, T.K. Lu, O.L. Franco, Antimicrobial peptides: role in human disease and potential as immunotherapies, Pharmacol. Ther. 178 (2017) 132–140, https://doi.org/10.1016/J.PHARMTHERA.2017.04.002.
[13] S. Gonçalves, P.M. Silva, M.R. Felício, L.N. de Medeiros, E. Kurtenbach, N.C. Santos, Psd1 effects on Candida albicans planktonic cells and biofilms, Front. Cell. Infect. Microbiol. 7 (2017) 249, , https://doi.org/10.3389/fcimb.2017.00249.
[14] M.E. Pachón-Ibáñez, Y. Smani, J. Pachón, J. Sánchez-Céspedes, Perspectives for clinical use of engineered human host defense antimicrobial peptides, FEMS Microbiol. Rev. 41 (2017) 323–342, https://doi.org/10.1093/femsre/fux012.
[15] A. De Breij, M. Riool, R.A. Cordfunke, N. Malanovic, L. De Boer, R.I. Koning, E. Ravensbergen, M. Franken, T. Van Der Heijde, B.K. Boekema, P.H.S. Kwakman, N. Kamp, A. El Ghalbzouri, K. Lohner, S.A.J. Zaat, J.W. Drijfhout, P.H. Nibbering, The antimicrobial peptide SAAP-148 combats drug-resistant bacteria and biofilms, Sci. Transl. Med. 10 (2018), https://doi.org/10.1126/scitranslmed.aan4044.
[16] M. Soethoudt, M.W.H. Hoorens, W. Doelman, A. Martella, M. van der Stelt, L.H. Heitman, Structure-kinetic relationship studies of cannabinoid CB 2 receptor agonists reveal substituent-specific lipophilic effects on residence time, Biochem. Pharmacol. (2018), https://doi.org/10.1016/j.bcp.2018.03.018.
[17] W.F. Porto, I.C.M. Fensterseifer, S.M. Ribeiro, O.L. Franco, Joker: an algorithm to insert patterns into sequences for designing antimicrobial peptides, Biochim. Biophys. Acta (2018) 1862, https://doi.org/10.1016/J.BBAGEN.2018.06.011.
[18] I.Y. Hirata, M.H. Sedenho Cezari, C.R. Nakaie, P. Boschcov, A.S. Ito, M.A. Juliano, L. Juliano, Internally quenched fluorogenic protease substrates: solid-phase synthesis and fluorescence spectroscopy of peptides containing ortho-aminobenzoyl/dinitrophenyl groups as donor-acceptor pairs, Lett. Pept. Sci. 1 (1995) 299–308, https://doi.org/10.1007/BF00119771.
[19] L.D. Mayer, M.J. Hope, P.R. Cullis, Vesicles of variable sizes produced by a rapid extrusion procedure, Biochim. Biophys. Acta 858 (1986) 161–168, https://doi.org/10.1016/0005-2736(86)90302-0.
[20] D.E. Warschawski, A.A. Arnold, M. Beaugrand, A. Gravel, É. Chartrand, I. Marcotte, Choosing membrane mimetics for NMR structural studies of transmembrane proteins, Biochim. Biophys. Acta 1808 (2011) 1957–1974, https://doi.org/10.1016/J.BBAMEM.2011.03.016.
[21] C.S. Alves, M.N. Melo, H.G. Franquelim, R. Ferre, M. Planas, L. Feliu, E. Bardají, W. Kowalczyk, D. Andreu, N.C. Santos, M.X. Fernandes, M.A.R.B. Castanho, E. Bardaji, W. Kowalczyk, D. Andreu, N.C. Santos, M.X. Fernandes, M.A.R.B. Castanho, Escherichia coli cell surface perturbation and disruption induced by antimicrobial peptides BP100 and pepR, J. Biol. Chem. 285 (2010) 27536–27544, https://doi.org/10.1074/jbc.M110.130955.
[22] O.N. Silva, I.C.M. Fensterseifer, E.A. Rodrigues, H.H.S. Holanda, N.R.F. Novaes, J.P.A. Cunha, T.M.B. Rezende, K.G. Magalhães, S.E. Moreno, M.S. Jerônimo, A.L. Bocca, O.L. Franco, Clavanin A improves outcome of complications from different bacterial infections, Antimicrob. Agents Chemother. 59 (2015) 1620–1626, https://doi.org/10.1128/AAC.03732-14.
[23] G.S. Bignami, A rapid and sensitive hemolysis neutralization assay for palytoxin, Toxicon 31 (1993) 817–820 http://www.sciencedirect.com/science/article/pii/004101019390389Z.
[24] I. Wiegand, K. Hilpert, R.E.W. Hancock, Agar and broth dilution methods to determine the minimal inhibitory concentration (MIC) of antimicrobial substances, Nat. Protoc. 3 (2008) 163–175, https://doi.org/10.1038/nprot.2007.521.
[25] L. Steinstraesser, T. Hirsch, M. Schulte, M. Kueckelhaus, F. Jacobsen, E.A. Mersch, I. Stricker, N. Afacan, H. Jenssen, R.E.W. Hancock, J. Kindrachuk, Innate defense regulator peptide 1018 in wound healing and wound infection, PLoS One 7 (2012) e39373, , https://doi.org/10.1371/journal.pone.0039373.
[26] W.F. Porto, L. Irazazabal, E.S.F. Alves, S.M. Ribeiro, C.O. Matos, Á.S. Pires, I.C.M. Fensterseifer, V.J. Miranda, E.F. Haney, V. Humblot, M.D.T. Torres, R.E.W. Hancock, L.M. Liao, A. Ladram, T.K. Lu, C. de la Fuente-Nunez, O.L. Franco, In silico optimization of a guava antimicrobial peptide enables combinatorial exploration for peptide design, Nat. Commun. 9 (2018) 1490, , https://doi.org/10.1038/s41467-018-03746-3.
[27] F. Reffuveille, C. de la Fuente-Núñez, S. Mansour, R.E.W. Hancock, A broad-spectrum antibiofilm peptide enhances antibiotic action against bacterial biofilms, Antimicrob. Agents Chemother. 58 (2014) 5363–5371, https://doi.org/10.1128/AAC.03163-14.
[28] L. Migliolo, M.R. Felício, M.H. Cardoso, O.N. Silva, M.-A.E. Xavier, D.O. Nolasco, A.S. de Oliveira, I. Roca-Subira, J. Vila Estape, L.D. Teixeira, S.M. Freitas, A.J. Otero-Gonzalez, S. Gonçalves, N.C. Santos, O.L. Franco, Structural and functional evaluation of the palindromic alanine-rich antimicrobial peptide Pa-MAP2, Biochim. Biophys. Acta 1858 (2016) 1488–1498, https://doi.org/10.1016/j.

bbamem.2016.04.003.
[29] M.H. Cardoso, S.M. Ribeiro, D.O. Nolasco, C. de la Fuente-Núñez, M.R. Felício, S. Gonçalves, C.O. Matos, L.M. Liao, N.C. Santos, R.E.W. Hancock, O.L. Franco, L. Migliolo, A polyalanine peptide derived from polar fish with anti-infectious activities, Sci. Rep. 6 (2016) 21385, , https://doi.org/10.1038/srep21385.
[30] L.D. Teixeira, O.N. Silva, L. Migliolo, I.C.M. Fensterseifer, O.L. Franco, In vivo antimicrobial evaluation of an alanine-rich peptide derived from Pleuronectes americanus, Peptides. 42 (2013), https://doi.org/10.1016/j.peptides.2013.02.001.
[31] K. Pane, V. Cafaro, A. Avitabile, M.D.T. Torres, A. Vollaro, E. De Gregorio, M.R. Catania, A. Di Maro, A. Bosso, G. Gallo, A. Zanfardino, M. Varcamonti, E. Pizzo, A. Di Donato, T.K. Lu, C. de la Fuente-Nunez, E. Notomista, Identification of novel cryptic multifunctional antimicrobial peptides from the human stomach enabled by a computational–experimental platform, ACS Synth. Biol. 7 (2018) 2105–2115, https://doi.org/10.1021/acssynbio.8b00084.
[32] M.M. Domingues, M.A.R.B. Castanho, N.C. Santos, rBPI21 promotes lipopolysaccharide aggregation and exerts its antimicrobial effects by (hemi)fusion of PG-containing membranes, PLoS One 4 (2009) e8385, , https://doi.org/10.1371/journal.pone.0008385.
[33] S.W. Provencher, CONTIN: a general purpose constrained regularization program for inverting noisy linear algebraic and integral equations, Comput. Phys. Commun. 27 (1982) 229–242, https://doi.org/10.1016/0010-4655(82)90174-6.
[34] J.M. Freire, M.M. Domingues, J. Matos, M.N. Melo, A.S. Veiga, N.C. Santos, M.A.R.B. Castanho, Using zeta-potential measurements to quantify peptide partition to lipid membranes, Eur. Biophys. J. 40 (2011) 481–487, https://doi.org/10.1007/s00249-010-0661-4.
[35] P.M. Carvalho, M.R. Felício, N.C. Santos, S. Gonçalves, M.M. Domingues, Application of light scattering techniques to nanoparticle characterization and development, Front. Chem. 6 (2018) 237, , https://doi.org/10.3389/fchem.2018.00237.
[36] E. Gross, R.S. Bedlack, L.M. Loew, Dual-wavelength ratiometric fluorescence measurement of the membrane dipole potential, Biophys. J. 67 (1994) 208–216, https://doi.org/10.1016/S0006-3495(94)80471-0.
[37] A. Hollmann, P.M. Matos, M.T. Augusto, M.A.R.B. Castanho, N.C. Santos, Conjugation of cholesterol to HIV-1 fusion inhibitor C34 increases peptide-membrane interactions potentiating its action, PLoS One 8 (2013) e60302, , https://doi.org/10.1371/journal.pone.0060302.
[38] P.M. Matos, M.A.R.B. Castanho, N.C. Santos, HIV-1 fusion inhibitor peptides enfuvirtide and T-1249 interact with erythrocyte and lymphocyte membranes, PLoS One 5 (2010) e9830, , https://doi.org/10.1371/journal.pone.0009830.
[39] J. Cladera, P. O'Shea, Intramembrane molecular dipoles affect the membrane insertion and folding of a model amphiphilic peptide, Biophys. J. 74 (1998) 2434–2442, https://doi.org/10.1016/S0006-3495(98)77951-2.
[40] S. Gonçalves, J. Abade, A. Teixeira, N.C. Santos, Lipid composition is a determinant for human defensin hnp1 selectivity, Biopolymers 98 (2012) 313–321, https://doi.org/10.1002/bip.22088.
[41] A. Hollmann, M.A.R.B. Castanho, B. Lee, N.C. Santos, Singlet oxygen effects on lipid membranes: implications for the mechanism of action of broad-spectrum viral fusion inhibitors, Biochem. J. 459 (2014) 161–170, https://doi.org/10.1042/BJ20131058.
[42] A.F. Faustino, G.M. Guerra, R.G. Huber, A. Hollmann, M.M. Domingues, G.M. Barbosa, F.J. Enguita, P.J. Bond, M.A.R.B. Castanho, A.T. Da Poian, F.C.L. Almeida, N.C. Santos, I.C. Martins, Understanding dengue virus capsid protein disordered N-terminus and pep14-23-based inhibition, ACS Chem. Biol. 10 (2015) 517–526, https://doi.org/10.1021/cb500640t.
[43] N.J. Greenfield, Determination of the folding of proteins as a function of denaturants, osmolytes or ligands using circular dichroism, Nat. Protoc. 1 (2007) 2733–2741, https://doi.org/10.1038/nprot.2006.229.
[44] F. Delaglio, S. Grzesiek, G. Vuister, G. Zhu, J. Pfeifer, A. Bax, NMRPipe: a multidimensional spectral processing system based on UNIX pipes, J. Biomol. NMR 6 (1995) 277–293, https://doi.org/10.1007/BF00197809.
[45] B.A. Johnson, R.A. Blevins, NMR View: a computer program for the visualization and analysis of NMR data, J. Biomol. NMR 4 (1994) 603–614, https://doi.org/10.1007/BF00404272.
[46] K. Wüthrich, NMR of Proteins and Nucleic Acids, New York (1986).
[47] C. Schwieters, J. Kuszewski, G. Mariusclore, Using Xplor–NIH for NMR molecular structure determination, Prog. Nucl. Magn. Reson. Spectrosc. 48 (2006) 47–62, https://doi.org/10.1016/j.pnmrs.2005.10.001.
[48] T.J. Dolinsky, J.E. Nielsen, J.A. McCammon, N.A. Baker, PDB2PQR: an automated pipeline for the setup of Poisson-Boltzmann electrostatics calculations, Nucleic Acids Res. 32 (2004) W665–W667, https://doi.org/10.1093/nar/gkh381.
[49] N.A. Baker, D. Sept, S. Joseph, M.J. Holst, J.A. McCammon, Electrostatics of nanosystems: application to microtubules and the ribosome, Proc. Natl. Acad. Sci. U. S. A. 98 (2001) 10037–10041, https://doi.org/10.1073/pnas.181342398.
[50] M.J. Frias, J. Melo-Cristino, M. Ramirez, The autolysin LytA contributes to efficient bacteriophage progeny release in Streptococcus pneumoniae, J. Bacteriol. 191 (2009) 5428–5440, https://doi.org/10.1128/JB.00477-09.
[51] P.M. Matos, H.G. Franquelim, M.A.R.B. Castanho, N.C. Santos, Quantitative assessment of peptide-lipid interactions. Ubiquitous fluorescence methodologies, Biochim. Biophys. Acta Biomembr. 1798 (2010) 1999–2012, https://doi.org/10.1016/j.bbamem.2010.07.012.
[52] P.M. Matos, S. Gonçalves, N.C. Santos, Interaction of peptides with biomembranes assessed by potential-sensitive fluorescent probes, J. Pept. Sci. 14 (2008) 407–415, https://doi.org/10.1002/psc.1005.
[53] D. Shang, Q. Zhang, W. Dong, H. Liang, X. Bi, The effects of LPS on the activity of Trp-containing antimicrobial peptides against Gram-negative bacteria and endotoxin neutralization, Acta Biomater. 33 (2016) 153–165, https://doi.org/10.1016/j.actbio.2016.01.019.
[54] A.H. Delcour, Outer membrane permeability and antibiotic resistance, Biochim. Biophys. Acta 1794 (2009) 808–816, https://doi.org/10.1016/J.BBAPAP.2008.11.005.
[55] A. Lisi, D. Pozzi, S. Grimaldi, Use of the fluorescent probe Laurdan to investigate structural organization of the vesicular stomatitis virus (VSV) membrane, Membr. Biochem. 10 (1993) 203–212, https://doi.org/10.3109/09687689309150268.
[56] D. Voss, T.J. Montville, 1,6-Diphenyl-1,3,5-hexatrine as a reporter of inner spore membrane fluidity in Bacillus subtilis and Alicyclobacillus acidoterrestris, J. Microbiol. Methods 96 (2014) 101–103, https://doi.org/10.1016/j.mimet.2013.11.009.
[57] K.S. Usachev, S.V. Efimov, O.A. Kolosova, A.V. Filippov, V.V. Klochkov, High-resolution NMR structure of the antimicrobial peptide protegrin-2 in the presence of DPC micelles, J. Biomol. NMR 61 (2015) 227–234, https://doi.org/10.1007/s10858-014-9885-4.
[58] B. Legrand, M. Laurencin, J. Sarkis, E. Duval, L. Mouret, J.F. Hubert, M. Collen, V. Vié, C. Zatylny-Gaudin, J. Henry, M. Baudy-Floc'H, A. Bondon, Structure and mechanism of action of a de novo antimicrobial detergent-like peptide, Biochim. Biophys. Acta (2011), https://doi.org/10.1016/j.bbamem.2010.08.020.
[59] K. Wüthrich, G. Wider, G. Wagner, W. Braun, Sequential resonance assignments as a basis for determination of spatial protein structures by high resolution proton nuclear magnetic resonance, J. Mol. Biol. 155 (1982) 311–319, https://doi.org/10.1016/0022-2836(82)90007-9.
[60] D.S. Wishart, B.D. Sykes, F.M. Richards, The chemical shift index: a fast and simple method for the assignment of protein secondary structure through NMR spectroscopy, Biochemistry (1992), https://doi.org/10.1021/bi00121a010.
[61] D.S. Wishart, B.D. Sykes, F.M. Richards, Relationship between nuclear magnetic resonance chemical shift and protein secondary structure, J. Mol. Biol. (1991), https://doi.org/10.1016/0022-2836(91)90214-Q.
[62] G.N. Ramachandran, C. Ramakrishnan, V. Sasisekharan, Stereochemistry of polypeptide chain configurations, J. Mol. Biol. (1963), https://doi.org/10.1016/S0022-2836(63)80023-6.
[63] M. McKenna, Antibiotic resistance: the last resort, Nature 499 (2013) 394–396, https://doi.org/10.1038/499394a.
[64] S.M. Ribeiro, M.R. Felício, E.V. Boas, S. Gonçalves, F.F. Costa, R.P. Samy, N.C. Santos, O.L. Franco, New frontiers for anti-biofilm drug development, Pharmacol. Ther. 160 (2016) 133–144, https://doi.org/10.1016/J.PHARMTHERA.2016.02.006.
[65] C. de la Fuente-Núñez, M.H. Cardoso, E. de Souza Cândido, O.L. Franco, R.E.W. Hancock, Synthetic antibiofilm peptides, Biochim. Biophys. Acta Biomembr. 1858 (2016) 1061–1069, https://doi.org/10.1016/J.BBAMEM.2015.12.015.
[66] N.B. da Cunha, N.B. Cobacho, J.F.C. Viana, L.A. Lima, K.B.O. Sampaio, S.S.M. Dohms, A.C.R. Ferreira, C. de la Fuente-Núñez, F.F. Costa, O.L. Franco, S.C. Dias, The next generation of antimicrobial peptides (AMPs) as molecular therapeutic tools for the treatment of diseases with social and economic impacts, Drug Discov. Today 22 (2017) 234–248, https://doi.org/10.1016/J.DRUDIS.2016.10.017.
[67] M.N. Gabere, W.S. Noble, Empirical comparison of web-based antimicrobial peptide prediction tools, Bioinformatics. 33 (2017) 1921–1929, https://doi.org/10.1093/bioinformatics/btx081.
[68] H.-T. Lee, C.-C. Lee, J.-R. Yang, J.Z.C. Lai, K.Y. Chang, A large-scale structural classification of antimicrobial peptides, Biomed. Res. Int. 2015 (2015) 1–6, https://doi.org/10.1155/2015/475062.
[69] F.H. Waghu, R.S. Barai, P. Gurung, S. Idicula-Thomas, CAMP$_{R3}$: a database on sequences, structures and signatures of antimicrobial peptides: Table 1, Nucleic Acids Res. 44 (2016) D1094–D1097, https://doi.org/10.1093/nar/gkv1051.
[70] S. Lata, B. Sharma, G. Raghava, Analysis and prediction of antibacterial peptides, BMC Bioinformatics 8 (2007) 263, https://doi.org/10.1186/1471-2105-8-263.
[71] S. Lata, N.K. Mishra, G.P. Raghava, AntiBP2: improved version of antibacterial peptide prediction, BMC Bioinformatics 11 (2010) S19, https://doi.org/10.1186/1471-2105-11-S1-S19.
[72] X. Wu, Z. Wang, X. Li, Y. Fan, G. He, Y. Wan, C. Yu, J. Tang, M. Li, X. Zhang, H. Zhang, R. Xiang, Y. Pan, Y. Liu, L. Lu, L. Yang, In vitro and in vivo activities of antimicrobial peptides developed using an amino acid-based activity prediction method, Antimicrob. Agents Chemother. 58 (2014) 5342–5349, https://doi.org/10.1128/AAC.02823-14.
[73] A. Barreto-Santamaría, H. Curtidor, G. Arévalo-Pinzón, C. Herrera, D. Suárez, W.H. Pérez, M.E. Patarroyo, A new synthetic peptide having two target of antibacterial action in E. coli ML35, Front. Microbiol. 7 (2016) 2006, , https://doi.org/10.3389/fmicb.2016.02006.
[74] P.B. Noto, G. Abbadessa, M. Cassone, G.D. Mateo, A. Agelan, J.D. Wade, D. Szabo, B. Kocsis, K. Nagy, F. Rozgonyi, L. Otvos Jr., Alternative stabilities of a proline-rich antibacterial peptide in vitro and in vivo, Protein Sci. 17 (2008) 1249–1255, https://doi.org/10.1110/ps.034330.108.
[75] P.Y. Muller, M.N. Milton, The determination and interpretation of the therapeutic index in drug development, Nat. Rev. Drug Discov. 11 (2012) 751–761, https://doi.org/10.1038/nrd3801.
[76] O.N. Silva, C. De La Fuente-Núñez, E.F. Haney, I.C.M. Fensterseifer, S.M. Ribeiro, W.F. Porto, P. Brown, C. Faria-Junior, T.M.B. Rezende, S.E. Moreno, T.K. Lu, R.E.W. Hancock, O.L. Franco, An anti-infective synthetic peptide with dual antimicrobial and immunomodulatory activities, Sci. Rep. 6 (2016) 35465, , https://doi.org/10.1038/srep35465.
[77] P.-K. Lai, Y.N. Kaznessis, Insights into membrane translocation of protegrin antimicrobial peptides by multistep molecular dynamics simulations, ACS Omega 3 (2018) 6056–6065, https://doi.org/10.1021/acsomega.8b00483.
[78] J.P. Ulmschneider, Charged antimicrobial peptides can translocate across

membranes without forming channel-like pores, Biophys. J. 113 (2017) 73–81, https://doi.org/10.1016/j.bpj.2017.04.056.
[79] R.M.R.F. Epand, R.M.R.F. Epand, Lipid domains in bacterial membranes and the action of antimicrobial agents, Biochim. Biophys. Acta 1788 (2009) 289–294, https://doi.org/10.1016/J.BBAMEM.2008.08.023.
[80] L.D. Renner, D.B. Weibel, Cardiolipin microdomains localize to negatively curved regions of Escherichia coli membranes, Proc. Natl. Acad. Sci. 108 (2011) 6264–6269, https://doi.org/10.1073/pnas.1015757108.
[81] R. Rashid, M. Veleba, K.A. Kline, Focal targeting of the bacterial envelope by antimicrobial peptides, Front. Cell Dev. Biol. 4 (2016) 55, https://doi.org/10.3389/fcell.2016.00055.
[82] E. Mileykovskaya, W. Dowhan, Cardiolipin-dependent formation of mitochondrial respiratory supercomplexes, Chem. Phys. Lipids 179 (2014) 42–48, https://doi.org/10.1016/J.CHEMPHYSLIP.2013.10.012.
[83] E. Mileykovskaya, W. Dowhan, Visualization of phospholipid domains in Escherichia coli by using the cardiolipin-specific fluorescent dye 10-N-nonyl acridine orange, J. Bacteriol. 182 (2000) 1172–1175, https://doi.org/10.1128/JB.182.4.1172-1175.2000.
[84] R. Koebnik, K.P. Locher, P. Van Gelder, Structure and function of bacterial outer membrane proteins: barrels in a nutshell, Mol. Microbiol. 37 (2000) 239–253, https://doi.org/10.1046/j.1365-2958.2000.01983.x.
[85] L. Zhang, P. Dhillon, H. Yan, S. Farmer, R.E. Hancock, Interactions of bacterial cationic peptide antibiotics with outer and cytoplasmic membranes of Pseudomonas aeruginosa, Antimicrob. Agents Chemother. 44 (2000) 3317–3321, https://doi.org/10.1128/AAC.44.12.3317-3321.2000.
[86] N.J. Greenfield, Using circular dichroism spectra to estimate protein secondary structure, Nat. Protoc. 1 (2007) 2876–2890, https://doi.org/10.1038/nprot.2006.202.
[87] É. Forde, G. Shafiy, D. Fitzgerald-Hughes, A.A. Strömstedt, M. Devocelle, Action of antimicrobial peptides and their prodrugs on model and biological membranes, J. Pept. Sci. (2018) e3086, , https://doi.org/10.1002/psc.3086.
[88] M.-C. Gagnon, E. Strandberg, A. Grau-Campistany, P. Wadhwani, J. Reichert, J. Bürck, F. Rabanal, M. Auger, J.-F. Paquin, A.S. Ulrich, Influence of the length and charge on the activity of α-helical amphipathic antimicrobial peptides, Biochemistry 56 (2017) 1680–1695, https://doi.org/10.1021/acs.biochem.6b01071.
[89] O.G. Travkova, H. Moehwald, G. Brezesinski, The interaction of antimicrobial peptides with membranes, Adv. Colloid Interf. Sci. 247 (2017) 521–532, https://doi.org/10.1016/J.CIS.2017.06.001.
[90] G.P.B. Carretero, G.K.V. Saraiva, A.C.G. Cauz, M.A. Rodrigues, S. Kiyota, K.A. Riske, A.A. dos Santos, M.F. Pinatto-Botelho, M.P. Bemquerer, F.J. Gueiros-Filho, H. Chaimovich, S. Schreier, I.M. Cuccovia, Synthesis, biophysical and functional studies of two BP100 analogues modified by a hydrophobic chain and a cyclic peptide, Biochim. Biophys. Acta 1860 (2018) 1502–1516, https://doi.org/10.1016/J.BBAMEM.2018.05.003.
[91] M.M. Domingues, S.C.D.N. Lopes, N.C. Santos, A. Quintas, M.A.R.B. Castanho, Fold-unfold transitions in the selectivity and mechanism of action of the N-terminal fragment of the bactericidal/permeability-increasing protein (rBPI(21)), Biophys. J. 96 (2009) 987–996, https://doi.org/10.1016/j.bpj.2008.10.044.
[92] M. Datrie, M. Schumann, T. Wieprecht, A. Winkler, M. Beyermann, E. Krause, K. Matsuzaki, O. Murase, M. Bienert, Peptide helicity and membrane surface charge modulate the balance of electrostatic and hydrophobic interactions with lipid bilayers and biological membranes, Biochemistry (1996), https://doi.org/10.1021/bi960835f.
[93] Y. Shen, F. Delaglio, G. Cornilescu, A. Bax, TALOS+: a hybrid method for predicting protein backbone torsion angles from NMR chemical shifts, J. Biomol. NMR 44 (2009) 213–223, https://doi.org/10.1007/s10858-009-9333-z.
[94] R. Koradi, M. Billeter, K. Wüthrich, MOLMOL: a program for display and analysis of macromolecular structures, J. Mol. Graph. 14 (1996) 51–55, https://doi.org/10.1016/0263-7855(96)00009-4.